

Analysis and Calibration of Internal Flow Force of Ejector-Powered Engine Simulator System in Wind Tunnels

TANG Wei^{1*}, WU Chaojun², HU Buyuan²

1. School of Aeronautics, Northwestern Polytechnical University, Xi'an 710072, P.R. China;

2. Low Speed Aerodynamics Research Institute, China Aerodynamic Research and Development Center, Mianyang 621000, P.R. China

(Received 18 March 2019; revised 20 May 2019; accepted 15 July 2019)

Abstract: The ejector-powered engine simulator (EPES) system is an important piece of equipment in conducting an influence test of the intake and jet flow in low-speed wind tunnels. In this work, through the analysis of the structure and principle of EPES, three parts of the internal flow force were obtained, namely, the additional resistance before the inlet, the internal flow force in the inlet and the thrust produced by the ejector. On the assumption of one-dimensional isentropic adiabatic flow, the theoretical formulae for calculating the forces were derived according to the measured total pressure, static pressure and total temperature of the internal flow section. Subsequently, a calibration tank was used to calibrate the EPES system. On the basis of the characteristics of the EPES system, the process and method of its calibration were designed in detail, and the model installation interface of the calibration tank was reformed. By applying this method, the repeatability accuracy of the inlet flow rate calibration coefficient was less than 0.05%, whereas that of the exhaust flow rate and velocity was less than 0.1%. Upon the application of the calibration coefficients to the correction of the wind tunnel experiment data, the results showed good agreement with the numerical simulation results in terms of regularity and magnitude before stall, which validates the reasonableness and feasibility of the calibration method. Analysis of the calibration data also demonstrated the consistency in the variation law and trend between the theoretical calculation and actual measurement of internal flow force, further reflecting the rationality and feasibility of the theoretical calculation. Nevertheless, the numerical difference was large and further widened with a higher ejection flow rate mainly because of the accuracy of flow measurement and the inhomogeneity of internal flow. The thrust deflection angle of EPES is an important factor in correcting this issue. In particular, the thrust deflection angle becomes larger with small ejection flow and becomes smaller with an increase in flow rate, essentially exhibiting a general change of less than 10°.

Key words: low-speed wind tunnel; ejector-powered engine simulator; calibration tank; internal flow force; inlet; jet

CLC number: TN925

Document code: A

Article ID: 1005-1120(2019)05-0747-13

0 Introduction

The effects of the inlet, the jet and a coupling of both on the aerodynamic characteristics of modern jet aircraft become more apparent with the flying-wing layout and stealth design. Here the local flow field of the head and the tail is expected to change as the airflow of the aircraft power system passes through the inlet and tail nozzles. As a result, it is

difficult to ignore the corresponding influence on the lift, drag and moment characteristics of the aircraft^[1-3]. Real simulation of the flow around the aircraft can be achieved through a simultaneous intake/exhaust test, which is the main method to obtain the aerodynamic influence of the power system on the aircraft and which has gradually become an integral part of the aircraft wind tunnel test. For this test, the main purpose is to determine and optimise the in-

*Corresponding author, E-mail address: ttww8079@163.com.

How to cite this article: TANG Wei, WU Chaojun, HU Buyuan. Analysis and Calibration of Internal Flow Force of Ejector-Powered Engine Simulator System in Wind Tunnels[J]. Transactions of Nanjing University of Aeronautics and Astronautics, 2019, 36(5): 747-759.

<http://dx.doi.org/10.16356/j.1005-1120.2019.05.006>

teraction between the engine intake and the exhaust, as well as their influence on the aircraft's aerodynamic force.

In wind tunnel tests, turbine power simulator (TPS) and ejector-powered engine simulator (EPES) are the two commonly used power simulation devices, which, since their introduction in the 1960s, have gradually become an important piece of equipment for such experiments^[4-9]. More specifically, the TPS is often applied for the wind tunnel test of transport aircraft and passenger aircraft with a plug-in engine. Because of the large volume, it is difficult to use an embedded engine for the simulation. Thus, in essence, the EPES is the preferred engine simulator in the intake and exhaust of fighter jets and stealth aircraft for integrated wind tunnel tests^[10-12].

Moreover, during wind tunnel testing, the engine simulator replicates the intake and exhaust flow and brings additional force to the model. This force is generated by the intake and exhaust flow. As the flow passes through the engine simulator, as in the case of the internal flow of a real engine, it can be alternatively called an internal flow force. By principle, such force is the additional force introduced by the engine simulator; thus, it should be measured and calculated accurately during the test. An accurate model of the aerodynamic forces and intake and exhaust effects can be obtained by taking the internal flow force into account during data processing^[13-16].

On the basis of the analysis of the mechanism of the internal flow force, a one-dimensional (1D) isentropic adiabatic flow hypothesis can be employed to make a preliminary estimation of the internal flow force by relying on the measured total internal flow pressure, static pressure and total temperature. Herein, the more precise method is ground calibration, which requires a special calibration device for accurately measuring and calculating the intake and exhaust mass flow rate and force of the model, as well as for identifying the relationship that exists between both parameters. The results of the calibration are presumed to lay a foundation for wind tunnel tests to simulate the intake and exhaust effects

and to deduct the internal flow force in data processing. Calibration of TPS using a calibration tank has been substantially studied both at home and abroad. Thus, it is both reasonable and feasible to apply a calibration tank to EPES calibration after appropriate adaptability modification. Moreover, the calibration makes it possible to accurately identify the relationships between the ejection parameters, the intake and exhaust mass flow rates, and the internal flow force. Essentially, the intake and exhaust mass flow rates can be controlled by varying the ejection flow rate during the wind tunnel test, thereby resulting to a more accurate simulation of the intake and exhaust states. This further leads to a more accurate understanding of the influence of the intake and exhaust flow on the aerodynamic characteristics of the model during data processing, which enables the realisation of the objective of the dynamic simulation test.

1 EPES in Wind Tunnel Test

The engine accelerates the air, increases the aerodynamic energy, produces momentum changes and then generates thrust to push the aircraft to overcome resistance for flight. The EPES system is based on the principle of the ejector. First, the ejector air flow is generated by high-pressure gas, which drives the flow of air in the inlet and causes the effect of intake and exhaust, and then, the working state of the engine in the wind tunnel test can be simulated. Likewise, this simulator system can perform ventilation model test, inlet test, jet test and intake and exhaust effect test simultaneously.

1.1 Basic principle

A schematic diagram of the EPES system is shown in Fig.1. Here, the EPES system is installed

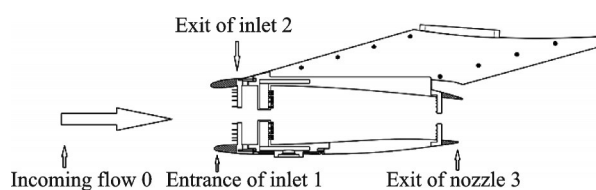


Fig.1 Schematic diagram of ejector propulsion simulation system

between the inlet and the nozzle. The air entering the inlet is accelerated by high-pressure air and is eliminated from the nozzle so that the intake and exhaust effects required in the wind tunnel test are obtained. Referring to the definition of aero engine, this part of airflow is called internal flow. Internal flow through the inlet and engine simulator and nozzle normally produces a corresponding internal flow force.

Accordingly, an internal flow plays two roles during the wind tunnel test. Firstly, the accelerated flow of the inlet and the nozzle affects the external flow field of the model, that is, the intake and exhaust effects that should be obtained for the wind tunnel test. Such influence is also the main purpose of the engine simulation test of the wind tunnel model. Secondly, it provides the internal flow force acting on the model. During the test, this part of the force is reflected in the measured data of the wind tunnel balance, together with the aerodynamic force of the model. Thus, it should be accurately defined and separated from the aerodynamic force data; otherwise, it would not be possible to obtain the influence of intake and exhaust effects on the aerodynamic performance of the model.

1.2 Structure

There are two installation modes of the EPES system on the wind tunnel model. The first mode describes the state where the simulator and the model are separated. The model is connected to the floating end of the balance, and the simulator is connected to the fixed end of the balance. In this condition, the internal flow force behind the inlet exit is not reflected in the wind tunnel balance load (Fig.2). The other mode is the state where the simulator and the model are integrated, and thus, the internal flow force and the outflow aerodynamic force are superimposed on the wind tunnel aerody-

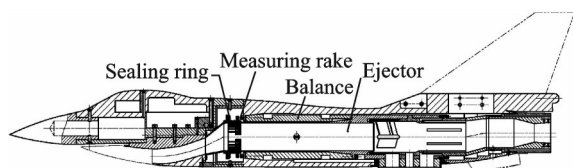


Fig.2 Separate ejector propulsion simulation system

dynamic balance load (Fig.3).

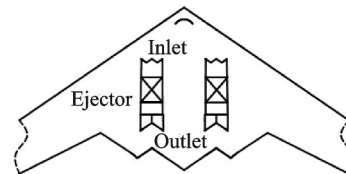


Fig.3 Integrated ejector propulsion simulation system

In a separated EPES system, the entrance of the simulator is connected to the exit of the aircraft inlet through a bellows, whereas the outlet of the simulator is connected to the nozzle. The model and the simulator are connected by a balance, and the high-pressure gas is connected to the simulator through the model support. In this state, the internal flow force produced by the simulator is not reflected in the balance load; however, the internal flow force of the inlet is reflected in the balance load, since the inlet is part of the model.

In an integrated EPES system, the simulator is designed as a part of the model, and high-pressure air is connected to the simulator through an air bridge. Therefore, the internal flow force generated by the simulator and the aerodynamic force generated by the outer surface of the model are both reflected in the balance load.

2 Analysis and Calculation of Internal Flow Force

A detailed analysis of the composition and calculation method of the internal flow force is the basis of wind tunnel experiment data correction. Therefore, with reference to the engine thrust division method in the analysis of the internal flow of an EPES system, the undisturbed wind tunnel inflow from the far front of the model to the exit of the model nozzle was taken as the analysis object.

2.1 Division of internal flow force

In Fig.1, the internal flow force can be divided into two parts from the exit of the wind tunnel model's inlet. Such classification is reasonable as the pressure rakes used to measure the total internal flow pressure and the static pressure are usually

installed at the inlet exit, and the ejection jet nozzle of the simulator is also positioned after the inlet exit. In order to ensure the authenticity of the internal flow in the inlet and thus reduce the flow interference, a test measuring device was not installed in the model inlet. At the same time, it is also helpful to carry out a test study of the inlet characteristics, along with the intake and exhaust influence test.

Before the exit of the model's inlet, the internal flow forces include the additional resistance in front of the inlet and the internal flow forces in the inlet. On one hand, the additional resistance before the inlet is the force exerted on the internal flow of the pre-entry pipe by the outflow. On the other hand, the internal flow of the pre-entry pipe flows from the far front to the inlet entrance. The additional resistance is due to the fact that, as a result of the difficulty of determining the flow parameters at the inlet entrance, the far front airflow is selected as the aircraft engine thrust calculation interface. The internal force of the inlet is produced by the internal flow on the inner wall of the model inlet and finally acts on model balance. Regardless of the EPES type, the additional resistance and internal flow force of the inlet are included in the balance force data, together with the aerodynamic force.

Behind the exit of the model's inlet, the internal flow force is basically the thrust generated by the ejection jet from the EPES system. That is, it is the force acting on the inner wall of the EPES system by the ejector primary airflow and the induced inlet airflow. When the EPES is separated with the wind tunnel model, this part of the force is not transmitted to the balance through the inner wall of the simulator; thus, it can be neglected. In the case of the EPES system that is integrated with the wind tunnel model, this part of the force is transmitted to the model balance and then becomes part of the balance measurement data.

2.2 Calculation of internal flow force

The internal flow force is similar to the thrust of the engine. It is difficult to calculate this force di-

rectly by means of the integral synthesis method. According to the momentum theorem, the internal flow force can be calculated to the momentum change rate of the air flow passing through the EPES system. This method does not only ignore the specific flow of air in the interior but also brings convenience to parameter measurement in the test. In the wind tunnel test, the total and static pressures of the air flow were measured by the pressure rake installed in the model inlet exit and in the nozzle exit. Fig.4 displays a pressure gauge rake, which is distributed along the radial direction of the inner flow channel.

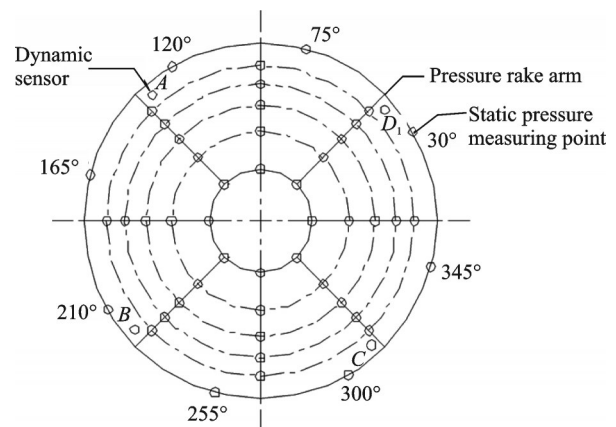


Fig.4 Schematic diagram of the pressure measurement rake and area block

The internal flow forces were calculated through the momentum equation. According to Fig.1, the following momentum equation was obtained

$$P_0 S_0 + \int_0^1 P dS + F'_{in} - P_3 S_3 = m_3 v_3 - m_0 v_0 \quad (1)$$

where P_0 is the atmospheric pressure, S_0 the pre-entry pipe cross-sectional area, m the air mass, v the air velocity and the subscripts represent occupancy (Fig.1). Moreover, F'_{in} is the internal flow force acting on the inner wall of the inlet and the simulator, and its reaction force F_{in} is the force acting on the test model by the internal flow and measured using the balance.

Since there are two ways to install the simulator, the force of internal flow was divided into two parts from the inlet exit. The momentum equations of these parts are as follows

$$P_2 S_2 + \int_0^1 P dS + F'_{in1} - P_2 S_2 = m_2 v_2 - m_0 v_0 \quad (2)$$

$$P_2 S_2 + F'_{in2} - P_3 S_3 = m_3 v_3 - m_2 v_2 \quad (3)$$

Of the different parameters presented, the reaction force F_{in1} of F'_{in1} is the internal flow force formed in the inlet, whereas the reaction force F_{in2} of F'_{in2} is the internal flow force formed in the simulator.

The measured parameters included the total and static pressures of the discrete points with equal area distribution on the sections of occupancies 2 and 3 in Fig.1. In the wind tunnel test, the approximate 1D isentropic flow aerodynamic equation was used to calculate the density, velocity and area of the pre-entry pipe before the inlet, which are then used to calculate the pressure and mass flow on the section. Consequently, the internal flow force was calculated according to the momentum equations above.

Pressure distributions at the inlet exit and nozzle exit sections are very different and uneven under different test conditions. If the average pressure and static pressure are used to calculate the measurement section pressure and mass flow, then the accuracy cannot be guaranteed. Alternatively, the method of discrete area synthesis is usually adopted^[17-22]. Here, the geometric area of the measurement section is subdivided into blocks as many as the measured points, which are the centre of each block. The pressure and mass flow of each block are calculated by taking the measured points' data as the average total pressure and static pressure of the block, and then, the pressure and flow of the whole section can be obtained by accumulating all of the blocks' data through the equation (with i as a measurement point)

$$PS = \sum_{i=1}^n P_i S_i \quad (4)$$

$$mv = \sum_{i=1}^n \rho_i v_i^2 S_i = \sum_{i=1}^n 2P_i S_i \times \frac{\kappa}{\kappa - 1} \left[\left(\frac{P_i}{P_i^*} \right)^{-\frac{\kappa}{\kappa - 1}} - 1 \right] \quad (5)$$

Therefore, the terms $m_2 v_2$, $m_3 v_3$, $P_2 S_2$ and $P_3 S_3$ can be calculated by measuring the section pa-

rameters, and then, the density and velocity of the corresponding section can be calculated by mass conservation equation and adiabatic isentropic flow hypothesis. Using these parameters, the internal flow force generated by the EPES system can be obtained according to Eq.(3).

Calculation of the additional resistance and the internal flow force formed by the inlet requires a certain transformation of Eq.(2). By taking advantage of the fact that the closed integral of atmospheric pressure along the surface of the control body is constant to zero, the control body from occupancies 0 to 1 in Fig. 1 is integrated to yield

$$P_0 S_1 + \int_0^1 P_0 dS - P_0 S_1 = 0 \quad (6)$$

Subsequently, Eq.(6) is considered into Eq.(2) to form

$$\int_0^1 (P - P_0) dS + F'_{in1} + P_0 S_1 - P_2 S_2 = m_2 v_2 - m_0 v_0 \quad (7)$$

In Eq.(7), the first integral is the additional resistance in front of the inlet, and the second term is the internal flow force of the inlet.

In a wind tunnel test, the required internal flow force can be calculated using Eqs.(3) and (7) by section measurement parameters and the installation form of the EPES system.

2.3 Further discussion on internal flow force

2.3.1 Axis of internal flow force

The effective thrust of an aero engine is the difference between the internal thrust and external resistance. The internal force of the EPES system is actually equivalent to the internal thrust of the aero engine. Therefore, the internal flow force, like the internal thrust of an aero engine, mainly acts on the axial direction of the EPES system. The formulae discussed in the preceding section are also derived from the axial direction. During the actual test, the calculated internal flow force should be decomposed into the balance coordinate system, according to the installation form of the EPES system, the angle of attack and the side slip angle.

2.3.2 Application of additional resistance

Additional resistance is the force acting on the pre-entry pipe in front of the inlet due to the defini-

tion of aero engine thrust. For an engine with an axisymmetric inlet, the additional resistance and the pressure distribution of the aero engine hood are collectively known as the total engine resistance. Under an ideal subsonic condition, according to Bernoulli equation, the pressure distribution of the aero engine hood forms a leading edge suction, which can just offset the additional resistance before the inlet. However, in practice, these two forces cannot be completely offset, and the remaining part is the overflow resistance. In particular, such additional resistance is closely related to the definition of thrust and resistance. Therefore, in actual wind tunnel tests, the use of additional resistance depends on circumstances. As shown in Figs.1, 5(a) and 5(b), if the model with engine simulator and ventilation model without simulator tests are compared to study the effects of intake and exhaust on the aerodynamic characteristics, the additional resistance should be deducted as part of the internal flow force in data processing. By contrast, the additional resistance should not be deducted as part of the internal flow force if the model with engine simulator tests is compared with the non-ventilated plugging cone model tests as the pressure of the far front flow in the cone plug model test directly acts on the cone plug. This part of the pressure is similar to additional resistance. Specifically, these pressure forces correspond to the internal flow forces of the pre-entry pipe before the inlet and therefore are included in the aerodynamic forces of the model.

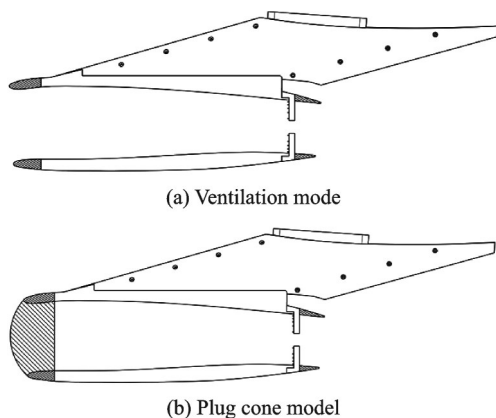


Fig.5 Propulsion simulation models

3 Calibration of Internal Flow Force

Internal flow force is calculated under the guidance of 1D approximate theory, along with an inherent calculation deviation. For TPS simulation systems in foreign countries, the calibration tank is usually used to calibrate the flow and thrust. There are four types of main calibration equipment, namely, the ECF calibration tank of the National Aerospace Laboratory of the Netherlands (NLR), the calibration tank of the British Aerospace Research Association, the calibration tank of the French Aerospace (ONERA) and the calibration tank of Boeing Company of the United States^[7,23-26]. In the past, an EPES system was calibrated in the wind tunnel without incoming flow; thus, its accuracy was relatively low. The shortcomings of the theoretical calculation and wind tunnel calibration were more distinct especially for the large S-bend and other unconventional inlet types of the engine simulation test. These were overcome by employing the principle and method of a calibration tank, which is one of the more accurate and feasible methods for measuring the intake and exhaust mass flow and calibrating the internal flow force of the EPES system.

3.1 Calibration experimental device

A calibration tank is a calibration test device for the power simulation system developed by Low-Speed Aerodynamics Research Institute of China Aerodynamic Research and Development Center (CARDC). The equipment consists of a calibration tank, a high-pressure air supply system, a high-pressure Venturi tube, a balance and air bridge, a low-pressure Venturi tube, a vacuum system, a measurement and monitoring system, and other subsystems. The calibration tank principle is illustrated in Fig.6.

Accordingly, the calibration of the EPES system is different from that of the TPS system in these areas:

(1) The EPES system has a single air passage, whereas the TPS system has a fan passage and a turbofan passage.

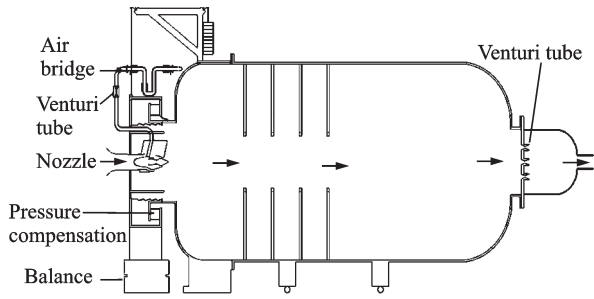


Fig.6 Schematic diagram of the CARDC calibration tank

(2) The EPES system is highly integrated with the wind tunnel model; thus, the simulator has to be redesigned for calibration. By contrast, the TPS system can be installed directly on the calibration tank.

3.2 Calibration process and method

The main parameters for calibrating the EPES system include the ejector primary flow rate, induced flow rate of the inlet, exhaust flow rate and the magnitude and angle of the internal flow force. The calibration process and method of the TPS system cannot be directly applied to the calibration of the EPES system. In this paper, the calibration process and method of EPES was established through an equipment analysis of the calibration tank and continuous experimental exploration. Fig.7 shows a chart of the basic process. In the calibration experiment, the actual flow rate m_{hp} of the high-pressure supply-gas was measured using a standard high-pressure Venturi flowmeter, and the total flow rate m_{tank} of the calibration tank was measured using a standard low-pressure Venturi flowmeter. The numerical difference between the two yields the actual EPES-induced flow rate of the inlet m_1 , that is

$$m_1 = m_{tank} - m_{hp} \quad (8)$$

and the exhaust flow rate, $m_j = m_{tank}$.

F_{thrust} is the thrust force and measured using the balance. According to the pressure and temperature measured by the sensor, through a 1D isentropic flow equation, the theoretical induced flow rate of the inlet $m_{1,id}$, exhaust flow rate $m_{j,id}$ and velocity $V_{j,id}$ could be calculated.

Accordingly, the calibration coefficients of EPES can be acquired using the following formula:

(1) Calibration coefficient of the induced flow rate of the inlet

$$Cd_1 = \frac{m_1}{m_{1,id}} \quad (9)$$

(2) Calibration coefficient of the exhaust flow rate

$$Cd_j = \frac{m_j}{m_{j,id}} \quad (10)$$

(3) Calibration coefficient of the exhaust flow velocity

$$Cv_j = \frac{F_{thrust}}{m_j \cdot V_{j,id}} \quad (11)$$

In wind tunnel experiments considering ejection, the theoretical induced flow rate of the inlet $m_{1,id}$, exhaust flow rate $m_{j,id}$ and velocity $V_{j,id}$ can be calculated based on the measured pressure and temperature of the model. Combining the above calibration coefficients makes it possible to compute the actual induced flow rate of the inlet m_1 , exhaust flow rate m_j and velocity V_j . Consequently, the actual thrust force of the model can be obtained.

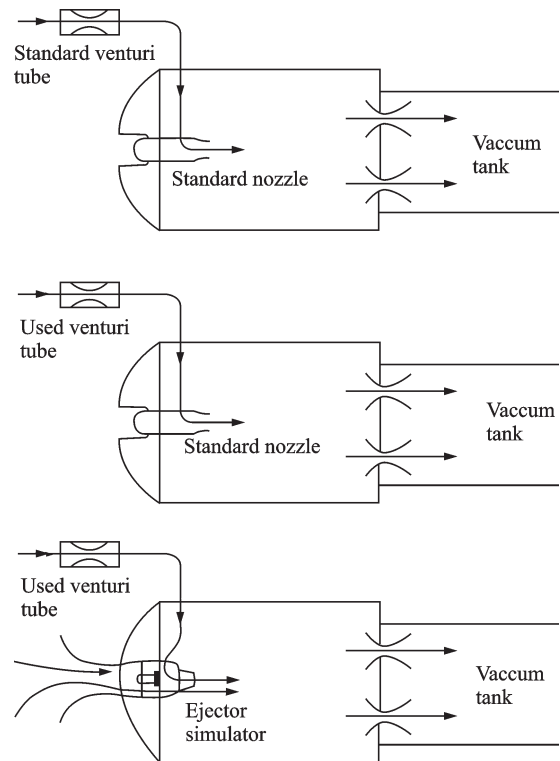


Fig.7 Schematic diagram of the calibration process

Nonetheless, the EPES system exhibits an inhomogeneous flow field, which results to a small angle between the nozzle jet and the nozzle axis, that

is, the angle between the internal flow force and the nozzle geometric axis. Thus, the deflection angle should be determined during calibration and taken into account in the data processing of wind tunnel test. The internal forces measured using the balance in the x -, y - and z -directions are F_x , F_y and F_z , respectively. The deflection angle of the forces can be expressed by

$$\delta_y = \arctan\left(\frac{F_y}{F_x}\right), \delta_z = \arctan\left(\frac{F_z}{F_x}\right) \quad (12)$$

3.3 Calibration data analysis

Fig.8 shows a structural diagram of the calibration model, with x representing the direction of air flow and y representing the vertical direction. This simulator system is installed in the flying-wing aircraft. Because of the embedded inlet and nozzle, a part of the fuselage section on the aircraft model is selected at the inlet entrance and at the nozzle exit of the calibration model to ensure that the calibration flow field coincides with the wind tunnel test. Moreover, the middle part of the model is located at the entrance of the calibration tank, and the front end is in an atmospheric environment. The nozzle exit of the back end is located in the calibration tank.

The test was carried out in the calibration tank of the Low-Speed Aerodynamics Institute, CARDC, as shown in Fig.9.

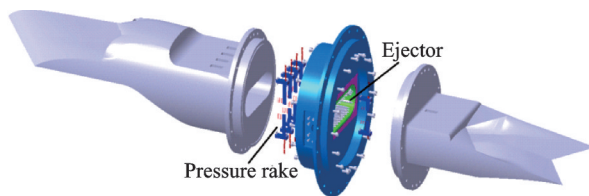


Fig.8 Structure of the calibration test model



Fig.9 Calibration test device

Further, the test had two states, namely, a ventilation state, where the simulator does not work, and an ejection state with a working simulator. Moreover, the test corresponded to the ventilation model test, whereas the engine simulation model test corresponded to the wind tunnel test.

Table 1 provides the calibration repeatability accuracy of the test. Under the same nozzle pressure ratio, the repeatability accuracy of the inlet flow rate calibration coefficient was less than 0.05%, and that of exhaust flow rate and velocity was less than 0.1%, which indicates that the flow field distortion at the measured cross-section was mainly a steady state under fixed experimental conditions. Likewise, the numerical difference between the measured value and the true value of the flow rate and velocity was constant, implying the feasibility of the calibration tank for the EPES system.

3.3.1 Ventilation state

Both the internal flow rate and the internal flow force were relatively small under the ventilation condition. As shown in Figs.10, 11 and 12, the inlet flow rate, internal flow force and z - and y -direction-

Table 1 Calibration repeatability accuracy

EPES condition	Ma	Nozzle pressure ratio	Theoretical induced flow rate of inlet/ ($\text{kg} \cdot \text{s}^{-1}$)	Repeatability		
				Cd_1	Cd_j	Cv_j
Without ejection	0.2	1.016	1.30	0.000 34	0.000 35	0.001 45
	0.3	1.038	1.93	0.000 35	0.000 26	0.001 00
	0.4	1.070	2.53	0.000 50	0.000 24	0.000 52
Ejection flow rate/ ($\text{kg} \cdot \text{s}^{-1}$)	0.5	1.101	2.05	0.000 45	0.000 18	0.000 99
	1.0	1.237	2.75	0.000 48	0.000 33	0.000 92
	1.5	1.428	3.23	0.000 45	0.000 21	0.000 79
	2.0	1.625	3.56	0.000 51	0.000 29	0.000 64

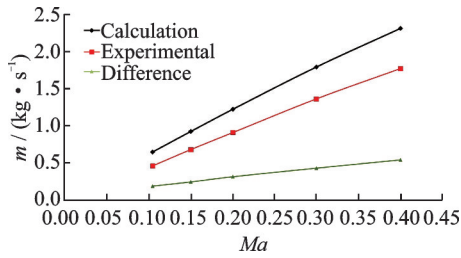


Fig.10 Inlet flow rate vs. Mach number

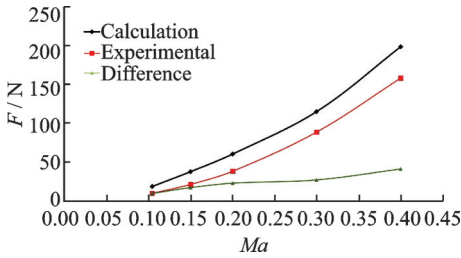


Fig.11 Internal flow force vs. Mach number

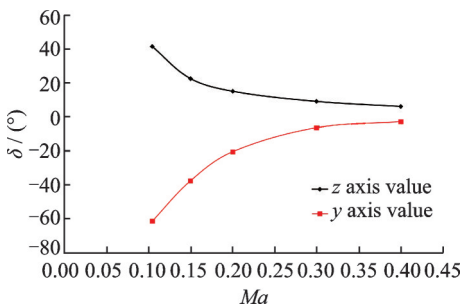


Fig.12 Internal flow force deflection angle vs. Mach number

force deflection angle varied with the Mach number of the calibration tank. Particularly in Figs. 10 and 11, the inlet flow rate and internal flow force increased with varying Mach number. On one hand, the inlet flow rate increased relatively slowly and then linearly increased in an approximate manner. On the other hand, the internal flow force increased rapidly, especially after the Mach number increased to 0.2.

Theoretical values of the inlet flow rate and internal flow force can be calculated from the total pressure and static pressure measured by the rake, whereas the actual value is obtained through the Venturi tube. The difference between the two values was obvious, and its magnitude increased as the Mach number increased, although the change was relatively slow. When the Mach number was 0.1, the difference between the values by theoretical calculation and actual measurement was almost the same. Moreover, the calculated internal force error

becomes very large under the condition of low Mach number. Further, with an increase in Mach number, the difference also increased, but with the ratio to the actual value becoming increasingly smaller along with a decreasing relative error.

The curve of the deflection angles of z and y varying with the Mach number is illustrated in Fig.12. From the diagram, note that the inhomogeneity of the internal flow induced a large deflection angle of force that influenced the measurement accuracy of the aerodynamic force and moment in the wind tunnel test. More specifically, the deflection angle decreased with an increasing Mach number, which reflects the homogeneity of the internal flow field. With an increase in velocity and flow rate, the flow became more and more uniform, the axial force increased, and the ratio of the lateral force to the axial force became increasingly smaller.

Two factors were accountable for the error of the theoretical and calculated values. The first reason is that the inlet and jet systems of the model were not simply axisymmetric; rather, both the inlet and the nozzle were S-shaped. As the theoretical calculation results of internal flow forces were based on the axisymmetric model under the assumption of a 1D flow, the calculated values were equivalent to the resultant forces measured using the balance. The actual measured value of the flow force in the model was the axial force in the x -direction and did not contain any lateral force. The second reason is the inhomogeneity of the flow field; The lower the velocity was, the greater the inhomogeneity of flow was and the smaller the axial force was. As such, the relative error of the theoretical calculation value was larger. Thus, an accurate calibration of the internal flow force is very essential to improve the accuracy of the intake and exhaust aerodynamic influence test with an EPES.

3.3.2 Ejection state

On the basis of the actual state of wind tunnel tests, equivalent Mach numbers of 0.2 and 0.15 were chosen to carry out the calibration experiment. When the Mach number is given, the pressure of the calibration box should be constant. This time, the nozzle pressure ratio of the EPES system is di-

rectly related to the ejection primary flow rate. Under the two Mach numbers, the simulator calibration tests were carried out in seven flow rate states of 0.5, 0.8, 1.0, 1.2, 1.5, 1.8 and 2.0 kg/s.

The curves of the internal flow forces varying with the ejector primary flow rate are shown in Figs. 13, 14 and 15. This internal force was measured using the balance in the x -direction of the simulator under different ejection flows, without considering the y - and z -direction forces. From the diagram, the variation of the internal flow force and the ejector primary flow rate exhibited a similar linear relationship. Similar to the inlet flow rate, there was a big difference between the theoretical and actual measurement values of the internal flow force. This difference further widened with an increase in

ejector primary flow rate, although the trend of change was basically the same. The difference between the measured values of the internal flow forces under two Mach numbers was small, which became increasingly smaller with an increase in the axial force. The maximum and minimum differences were 17 and 1 N forces, respectively. Essentially, the magnitude of the ejector primary flow rate could be regarded as the key determiner of the x -axial force.

Fig. 16 displays the relationship between the actual nozzle exit flow rate and the internal flow force. This diagram contains three curves: one without ejection and two with ejection and corresponding to Mach numbers of 0.2 and 0.15. Moreover, these curves accord with the theoretical relationship that the internal flow force is proportional to the square of the nozzle exit flow rate, with relatively concentrated data points and with high coincidence. Here, the fitting curve can be used to modify the model force data in the wind tunnel test when it is convenient and accurate to obtain the nozzle exit flow.

Fig. 17 depicts the relationship between the deflection angle of the z - and y -directions of the simulator and the ejector primary flow rate. Under the two

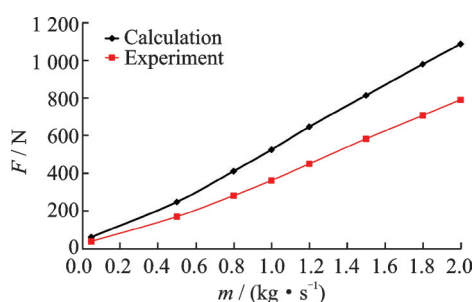


Fig. 13 Internal flow force vs. ejector primary flow rate ($Ma = 0.20$)

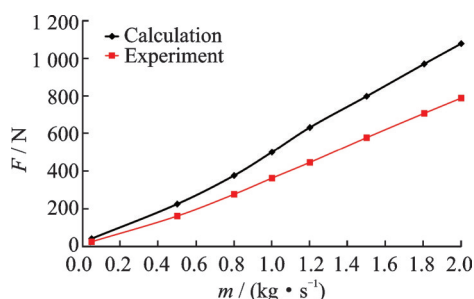


Fig. 14 Internal flow force vs. ejector primary flow rate ($Ma = 0.15$)

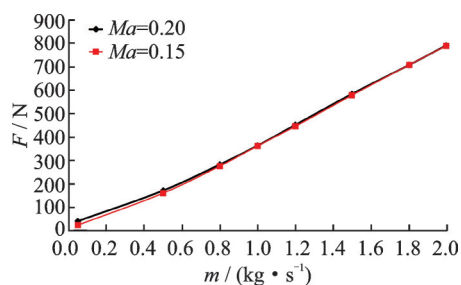


Fig. 15 Internal flow force vs. ejector primary flow rate ($Ma = 0.20, 0.15$)

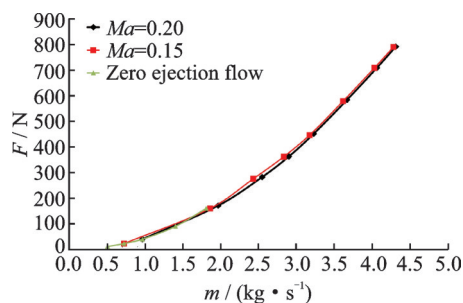


Fig. 16 Internal flow force vs. nozzle exit flow rate

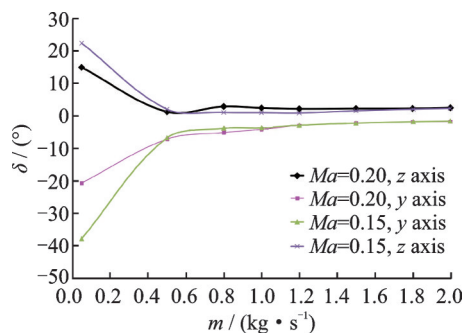


Fig. 17 Deflection angles of z - and y -axis forces vs. ejection flow

Mach numbers 0.20 and 0.15, the deflection angle of the y -direction force decreased with an increase in either the ejector primary flow rate or the internal flow force. On the contrary, the deflection angle of the z -direction force varied slightly and tended to be enhanced. From the magnitude of the numerical values, the z -direction deflection of the force was basically within 3° , and the deflection of the force in the y -direction was relatively large, within 10° . The magnitude of the z - and y -direction forces measured in the balance increased with greater ejector primary flow rate, as shown in Fig.18. Essentially, the variation of the z -direction force was relatively large and demonstrated a distinct jump with an increase in the ejector primary flow rate. The variation of the y -direction force was relatively stable and demonstrated a very slight change as the flow rate exceeded 1 kg/s and then basically remained constant. The z -direction force's change was larger and irregular, whereas that of the y -direction force was smaller with better regularity. This indicates apparent internal flow inhomogeneity, which especially became prominent in the z -direction. On the basis of the actual measurement results, the regularity of the z - and y -direction forces was not discernible, and the difference between the data points was large, which is expected to be an important factor for the final wind tunnel test data correction. Therefore, in order to ensure the accuracy of the data, each state of the simulator in the wind tunnel test should be calibrated in the calibration tank. It is equally recommended that the corresponding calibration data should be used when correcting the wind tunnel test data. By contrast, it is suggested that the difference and fitting methods should not be used in correcting the z - and y -direc-

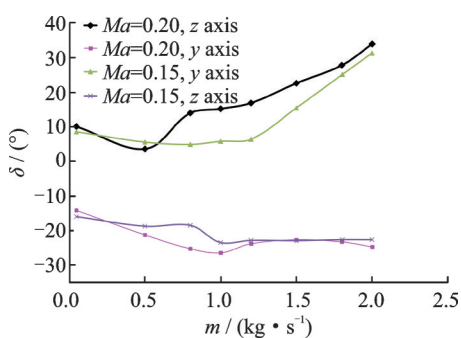


Fig.18 z - and y -axis forces vs. ejector flow

tion forces.

4 Application of Calibration Data in Wind Tunnel Experiment

One of the important purposes of engine simulation test is to obtain the influence of intake and exhaust on the aerodynamic force of a model, especially the disturbance to the model resistance. During the test, the balance load along the axis of the model included the additional resistance D_{ram} before the inlet, the internal flow force F_{in1} and the thrust F_{in2} of the EPES jet, the model resistance D_M without an engine simulator, and the interference resistance D_{jet} of the intake and exhaust to the model. The relationship among the variables is expressed as

$$F_{Load} = F_{in2} - D_{ram} - F_{in1} - D_M - D_{jet} \quad (13)$$

where F_{Load} is the x -direction force of the balance measurement and the resistance D_M of the model is the result of the test without an engine simulator in the same model state as that of the test with an engine simulator. Eq. (13) reflects that the influence D_{jet} of the EPES system on model resistance can be calculated. Here, the magnitude of the interference resistance accounts for approximately 1% of the internal flow force. Therefore, the accuracy of the calculation of the internal flow force and the resistance measurement in the EPES system is more challenging in achieving such objective. Similarly, the effect of the deflection angle of the internal flow force on the normal force and the lateral force should be deducted in data processing.

Fig.19 shows a comparison of drag coefficients between the data obtained from the numerical simu-

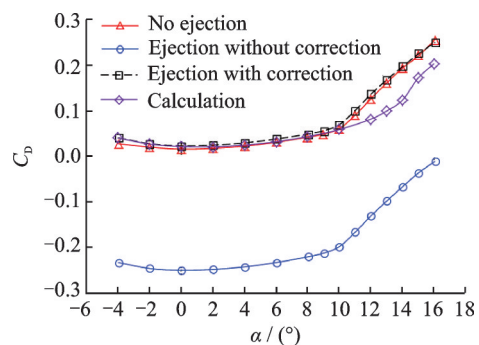


Fig.19 Typical drag characteristic with inlet and jet-effects testing

lation and experiments with calibration correction. Note that the experiment was carried out in the 8-m-long, 6-m-wide low-speed wind tunnel of CARDC using the calibrated EPES above.

Accordingly, the numerical simulation data were obtained with the same parameter conditions as the wind tunnel experiment. Without calibration correction, the drag coefficient was a large, negative value because the EPES thrust was much greater than the model drag. Upon the application of the calibration coefficients to the correction of the wind tunnel experiment data, the results demonstrated good agreement with the numerical simulation results in terms of regularity and magnitude before stall, as indicated in Fig. 19, thereby validating the reasonableness and feasibility of the calibration method.

5 Conclusions

The internal flow force is an important physical quantity that needs to be measured and calculated when an aircraft engine simulation test is carried out in the wind tunnel. In this study, the calculation and calibration method of this physical quantity was presented based on a detailed analysis of the internal force. Moreover, simulator calibration experiments were performed using a ground calibration device. The main findings of this study can be generalised as follows:

(1) This study made a detailed analysis of the composition of the internal flow force of EPES, as well as defined the calculation method of deducing the force in the wind tunnel experiment. The calibration flow and quantity calculation formula for calibrating the internal flow force with a calibration tank were determined through experiments.

(2) The inlet flow rate calibration coefficient demonstrated a repeatability accuracy of less than 0.05%, and that of exhaust flow rate and velocity was less than 0.1%. The results of the wind tunnel calibration were in good agreement with the numerical simulation results before the model stalled.

(3) The variation law and trend of the theoretical calculation were consistent with the actual mea-

surement of internal flow force, thereby reflecting the rationality and feasibility of the theoretical calculation. Nonetheless, the numerical difference was large, which further widened with a higher ejection flow rate. The thrust deflection angle of EPES was an important factor in correcting such difference, which cannot be obtained by theoretical calculation, but only through calibration.

(4) As a whole, the actual wind tunnel test verified the applicability of the calibration and analysis method of the internal flow force. The next step is to promote the utilisation of the method in wind tunnel testing.

References

- [1] ZHANG Jing, ZHANG Xiao Liang, JIANG Yi Ting. The research on aerodynamic characteristics of high-lift configuration of transport plane with the effect of engine jet[J]. *Aero Weaponry*, 2014(3): 28-31. (in Chinese)
- [2] YU Xinhua, TAO Yujin, ZHANG Lin, et al. Influence of engine inlet and exhaust on flying wing UAV and its mechanism analysis[J]. *Journal of Beijing University of Aeronautics and Astronautics*, 2015, 41(5): 786-792. (in Chinese)
- [3] LI Xiang, ZHAO Changxia, RONG Haichun. Analysis effects of the inlet-exhaust system on the flying wing UAV lift-drag characteristics[J]. *Journal of Xi'an Aeronautical University*, 2017, 35(1): 8-12. (in Chinese)
- [4] MCWATERS M. F-35 conventional mode jet-effects testing methodology[R]. AIAA-2005-2404, 2005.
- [5] NICOLOFF G B, WEBER H A. Characteristics of an ejector-type engine simulator for STOL model testing[R]. AIAA-1972-1028, 1972.
- [6] ROBINSON C E, SMITH G D, MATZ R J, et al. Evaluation of an ejector-powered engine simulator at transonic mach number[R]. AIAA-1979-1165, 1979.
- [7] KOOI J W, DE HAIJ L, HEGEN G H. Engine simulator with turbofan powered simulators in the German-Dutch wind tunnels[R]. AIAA-2002-2919, 2002.
- [8] BURGSMULLER W, SZODRUCH J. Benefits and costs of powered engine simulator at low speeds[R]. AIAA-1985-0381, 1985.
- [9] LEE J D, FREULER R J. Engine simulator techniques for scaled test cell studies[R]. AIAA-1985-1282, 1985.
- [10] WU Chaojun, NIE Bowen, KONG Peng, et al. Test technology on unsteady characteristics of inlet flow during fighter plane maneuvers[J]. *Journal of Experi-*

- ments in Fluid Mechanics, 2017, 31(2): 98-102. (in Chinese).
- [11] FAN Jianchao, HUA Jie, YU Kunlong, et al. A test technique for submerged inlet model in FL-24 wind tunnel[J]. Journal of Experiments in Fluid Dynamics, 2008, 22(1): 92-94. (in Chinese)
- [12] CHE Jiexian, YE Wei, SUN Haitao, et al. Experimental investigation of a full-scale inlet in ground running[J]. Gas Turbine Experiment and Research, 2014, 27(3):12-15. (in Chinese)
- [13] HAO Weidong, DENG Xueying, QU Fangliang. Simulated test technique for engine air intake and exhaust in high speed wind tunnel[J]. Journal of Beijing University of Aeronautics and Astronautics, 2005, 31(4): 459-463. (in Chinese)
- [14] ZHANG Rongping, WANG Xunnian, JING Rongchao. Development in ejector nacelle simulation testing in low speed wind tunnel[J]. Acta Aerodynamica Sinica, 2016, 34(6): 756-761. (in Chinese)
- [15] ZHANG Le, ZHOU Zhou, XU Xiao Ping, et al. Numerical simulation of power and flow field characteristics of conformal intake and exhaust for flying wing unmanned aerial vehicle[J]. Journal of Northwestern Polytechnical University, 2015, 33(3): 353-360. (in Chinese)
- [16] QU Fangliang, AN Ruoming, HAN Xiaotao, et al. The investigation of engine simulation test with ejector in high speed wind tunnel[J]. Experiments and Measurements in Fluid Mechanics, 2002, 16(3): 8-13. (in Chinese)
- [17] MA Yanrong. Development and experiment of jointed rake for airflow and boundary-layer measurement[J]. Gas Turbine Experiment and Research, 2014, 27(3): 54-58. (in Chinese)
- [18] ZHAO Haigang, SHEN Shicai, ZHANG Xiaofei, et al. Flight test of mass flow measurement of turbofan engine[J]. Journal of Aerospace Power, 2012, 27(8): 1778-1784. (in Chinese)
- [19] ZHANG Shaowu, GUAN Xiangdong, ZHU Tao, et al. Investigation on facts affecting the measurement accuracy for inlet flow coefficient in hypersonic tunnel[J]. Journal of Propulsion Technology, 2013, 34(4): 470-476. (in Chinese)
- [20] XU Zhulin, DA Xingya, FAN Zhaolin. Assessment of swirl distortion of serpentine inlet based on five-hole probe[J]. ACTA Aeronautica et Astronautica Sinica, 2017, 38(12):121342. (in Chinese)
- [21] SHI Jianbang, SHEN Shicai, GAO Yang, et al. Research on the aero-engine airflow measurement and calculation method[J]. Engineering & Test, 2011, 51(4): 15-18. (in Chinese)
- [22] OU Ping, CHEN Qiang, TIAN Xiaohu, et al. The pumping system and precise mass flow measuring technique for double-inlet wind tunnel test[J]. Acta Aerodynamica Sinica, 2016, 34(3): 392-397. (in Chinese)
- [23] LI Cong, XU Tiejun. Calibration and test for ejector and TPS[J]. Journal of Experiments in Fluid Dynamics, 2006, 20(1): 17-22. (in Chinese)
- [24] YI Bingli, ZENG Kai, WANG Shihong. Investigation on the interference correction of flying wing aircraft rear sting support in high speed wind tunnel test[J]. Acta Aerodynamica Sinica, 2016, 34(1): 98-106. (in Chinese)
- [25] PHILIPSEN L, HEGEN S. Advances in propeller simulation testing at the German-Dutch wind tunnel[R]. AIAA-2004-2502, 2004.
- [26] ZHANG Rongping, WANG Xunnian, HUANG Yong. Air bridge technology for engine power simulation test in wind tunnel[J]. Journal of Aerospace Power, 2015, 30(4): 910-915.

Acknowledgement This work was supported by the fundamental research the Funds of China Aerodynamics Research and Development Center. And the authors would like to acknowledge the following people for their assistance: ZHANG Rongping, LI Dong, LIANG Jian, and all with the Low-Speed Aerodynamics Institute of China Aerodynamics Research and Development Center.

Authors Dr. TANG Wei has long been engaged in the research of low-speed aerodynamic wind tunnel test technology. His main research direction is wind tunnel dynamic simulation of aircraft.

Mr. WU Chaojun is a senior researcher at the China Aerodynamics Research and Development Center. He is highly accomplished in the design, testing, and optimisation of engine inlets.

Mr. HU Buyuan is a senior researcher at the China Aerodynamics Research and Development Center. He has completed a large number of wind tunnel tests, and has made great achievements in aircraft engine simulation test.

Author contributions Dr. TANG Wei wrote the manuscript. Mr. WU Chaojun designed the research programme. Mr. HU Buyuan completed the wind tunnel test. All authors jointly completed the data analysis research and commented on the manuscript draft and approved the submission.

Conflicts interests The authors declare no competing interests.